



**HAL**  
open science

# Modelling of a PsD hybrid test on a RC column/beam junction combining a multifibre beam model and a POD-ROM approach

Bastien Bodnar, Walid Larbi, Magdalini Titirla, Jean-François Deü, Fabrice Gatuingt, Frédéric Ragueneau

► **To cite this version:**

Bastien Bodnar, Walid Larbi, Magdalini Titirla, Jean-François Deü, Fabrice Gatuingt, et al.. Modelling of a PsD hybrid test on a RC column/beam junction combining a multifibre beam model and a POD-ROM approach. Computational Modelling of Concrete Structures, Euro-C 2022, May 2022, Vienne, Austria. pp.414 - 423, 10.1201/9781003316404-49 . hal-03677950

**HAL Id: hal-03677950**

**<https://hal.science/hal-03677950v1>**

Submitted on 25 May 2022

**HAL** is a multi-disciplinary open access archive for the deposit and dissemination of scientific research documents, whether they are published or not. The documents may come from teaching and research institutions in France or abroad, or from public or private research centers.

L'archive ouverte pluridisciplinaire **HAL**, est destinée au dépôt et à la diffusion de documents scientifiques de niveau recherche, publiés ou non, émanant des établissements d'enseignement et de recherche français ou étrangers, des laboratoires publics ou privés.



Distributed under a Creative Commons Attribution - NonCommercial - NoDerivatives 4.0 International License

# Modelling of a PsD hybrid test on a RC column/beam junction combining a multifibre beam model and a POD-ROM approach

B. Bodnar, W. Larbi, M. Titirla & J.-F. Deü

*Conservatoire National des Arts et Métiers, Laboratoire de Mécanique des Structures et des Systèmes Couplés, Paris, France*

F. Gatuingt & F. Ragueneau

*Université Paris-Saclay, Centrale Supélec, ENS Paris-Saclay, CNRS, Laboratoire de Mécanique Paris-Saclay, Gif-sur-Yvette, France*

**ABSTRACT:** In this paper, a pseudo dynamic (PsD) hybrid experimental setup allows for assessing the nonlinear behaviour of a reinforced concrete (RC) column/beam junction under earthquake is proposed. The specimen is linked to a numerical substructure made of multifibre beam elements modelling the other parts of the building. To reduce the CPU time related to the numerical substructure, a proper orthogonal decomposition (POD) projection modal basis is computed from an offline implicit finite element analysis and used to reduce the size of the matrix system. A bilinear elastic-plastic law is used for steel rebars, and a unilateral damage law is used for concrete. Step-by-step calculations are performed using a non-iterative, unconditionally stable and explicit  $\alpha$ -OS splitting scheme during the hybrid test (*i.e.* the online phase). A substructuring method is applied to the column-beam junction located at the first-floor level. The reliability of the modelling assumptions as well as the use of POD-modes in the case of quasi-brittle materials are discussed. The analyses are performed by using MATLAB<sup>®</sup> software. In a first attempt, the column-beam junction response is computed using a 2D nonlinear numerical model defined in Cast3M<sup>®</sup> software. Results show that using a POD projection modal basis does not significantly reduce the computational cost when the  $\alpha$ -OS method is used but improves the response of both numerical and tested substructures thanks to the nonlinearities taken into account into the POD-modes.

## 1 INTRODUCTION

It is sometimes necessary to perform tests on structural elements to study their behaviour under seismic loading (damage, failure mechanisms, ...) in the civil engineering field. For this purpose, it is possible to carry out quasi-static “push-over” tests (consisting of stressing the specimen by applying step by step the shape of the first vibratory mode) or dynamic tests on a reduced specimen (on a shaking table or in a centrifuge facility). Although, even if these tests are commonly used, they have many limitations. It is impossible to consider the inertial and viscous forces in the first case. In the second one, the similitude theory leads to the addition of masses, sometimes leading to unrealistic collapse mechanisms due to local stresses.

To overcome these limitations, “hybrid tests” have been developed over the last few decades. They allow the assessment of the response of structural elements under seismic loading at full scale by considering the environment in which they are installed. The specimen is loaded at its ends by actuators whose displacements are computed through numerical calculations carried out simultaneously on a complete structure.

Displacements are applied at each time step by actuators, and the corresponding measured restoring forces are used as boundary conditions for the numerical substructure. The results give the displacements of actuators for the next time step and so on.

The key idea was introduced by Hakuno et al. (1969), who proposed solving the harmonic oscillator equation by measuring the restoring force of an embedded beam specimen in real-time. However, its study showed that many technical limitations related to the control and delay of actuators do not allow to perform the test in real-time. To overcome these limits, Takanashi et al. (1969) proposed to carry out Pseudo dynamic (PsD) hybrid tests. Actuators thus apply the displacements in deferred time. As a result, only the static restoring forces are measured, while the viscous damping and the inertial forces related to the tested substructure remain unknown. To assess them, Buchet et al. (1994) showed that it is possible to compute them numerically by adding the tested substructure to the numerical model. The specimen can thus be modelled on the common degrees of freedom (DOFs) by a nonlinear oscillator (semi-global approach) or by a complete numerical model (global approach). As a

result, the viscous damping and the inertial forces are assessed according to the measured restoring forces but depend on the damping applied numerically.

Performing dynamic finite element analyses in the framework of PsD hybrid tests requires specific non-iterative methods to avoid the risk of overshoot (*i.e.* sudden collapse of the specimen) as well as nonlinear material laws modelling the decrease of stiffness due to damage on the numerical substructure. Nakashima (1992) proposed to implement an Operator Splitting (OS) method to assess the nonlinear restoring forces. The vector is split into a nonlinear term computed from an explicit prediction and a linear term depending on the displacements on the time step. Thus, this scheme remains linearly implicit but becomes nonlinearly explicit, so iterations are unnecessary. The accuracy of this integration scheme, called  $\alpha$ -OS, was assessed by Combesure (1997), who showed its reliability when the loss of stiffness does not imply a significant shift in frequency of the high-frequency modes. The  $\alpha$ -OS method was later successfully applied by several researchers, including Pegon et al. (2000) and Souid (2009).

Carrying out real-time hybrid tests is still challenging due to many technical limitations related to the delay of the actuators and the computational cost required to solve the nonlinear numerical substructure. However, the CPU time can be reduced by using simplified models, such as macro elements (Moutousamy 2013), elastic-plastic hinges (Nguyen 2012), and multifibre beam elements (Lebon 2011), as well as reduced-order modelling (ROM) methods (POD-ROM, POD-DEIM, ...). To the best of our knowledge, the use of ROM on RC structures made of multifibre beam elements has not been investigated yet in the framework of hybrid tests.

Due to their highly nonlinear behaviour under earthquakes, several researchers performed quasi-static tests on column beam junctions (Iskef 2016). However, in the case of a PsD hybrid test, relevant boundary conditions need to be applied to the specimen to obtain valuable results. Thus, carrying PsD hybrid tests on RC column/beam junctions remains a challenging task.

In this paper, a PsD hybrid experimental setup allows for assessing the nonlinear behaviour of a RC column/beam junction under earthquake is proposed. The modelling of the numerical substructures (made of multifibre beam elements) is first described. The  $\alpha$ -OS time integration scheme and the substructuring method are then detailed. A POD projection modal basis (computed from the results of an offline finite element analysis) is also added to the procedure to reduce CPU time. Note that the experimental setup is not yet available in our research. The tested specimen is then replaced by a 2D numerical model defined in Cast3M<sup>©</sup> software. The reliability of POD projection modal bases in the case of hybrid tests is next assessed by comparison with the offline and full order model (FOM) solutions. The boundary conditions applied to the specimen are finally discussed based on the damage index distribution.

## 2 NONLINEAR MODELLING OF THE SUBSTRUCTURES

### 2.1 Timoshenko multifibre beam elements

The hybrid test framework requires low time-consuming analyses with numerical models taking account of the loss of stiffness due to damage on the numerical substructure. So, to correctly model the behaviour of RC elements under earthquake, a highly nonlinear “unilateral” damage law needs to be used for concrete. Thus, to ensure a quick convergence of the results and perform real-time or quick PsD hybrid tests, local scale models are usually not used. Semi-global approaches (multifibre beams and multilayer shells) are chosen instead (*cf.* Figure 1). They describe the global kinematic by using a beam (or shell) model whose integration points are linked to a section made of 1D nonlinear fibres (or layers). The deformation of each fibre (or layer) is assessed assuming that the beam cross-sections remain plane. Nonlinear damage laws are then used to update the properties of the fibres at each iteration. Generalized stresses are computed through a double integration: one on the sections and the other on the beam elements. Multifibre beams were previously used by Lebon (2011) to perform PsD hybrid tests on RC frames. In this work, the structure is modelled using the Timoshenko multifibre beam elements developed by Kotronis (2004).

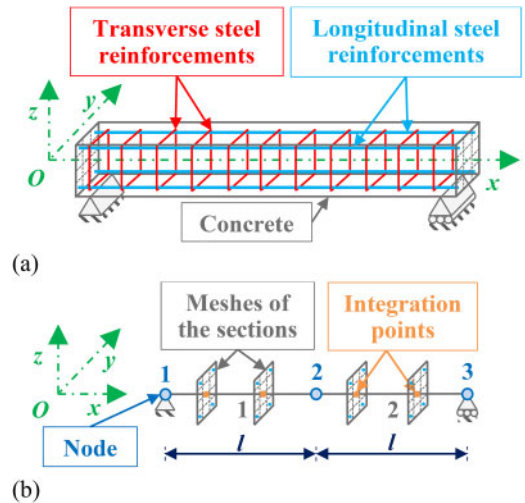


Figure 1. Simply supported RC beam on nodes 1 and 3 (a) and multifibre mesh with two Timoshenko beam elements (b).

### 2.2 Nonlinear material laws

In the case of hybrid tests, nonlinear material laws are required to model the decrease of stiffness due to damage during earthquakes. In addition, cyclic movements generate hardening of plastic steel rebars and opening/closing of cracks in damaged concrete, leading to

the appearance of a “unilateral” effect (*i.e.* progressive recovery of stiffness when the cracks are closing). Material laws modelling these phenomena are thus required.

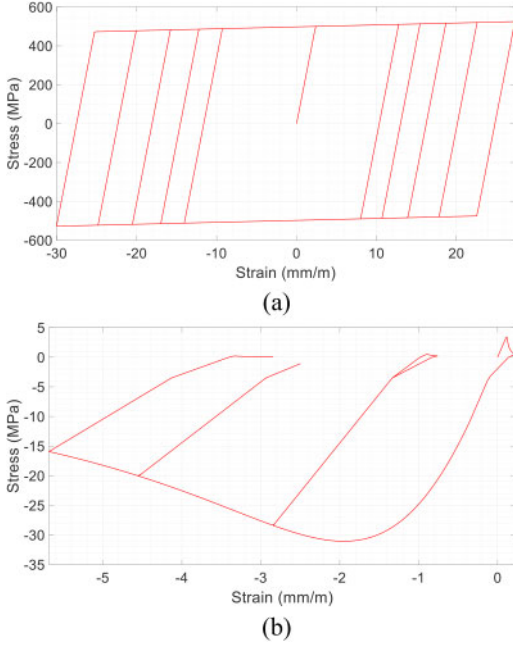


Figure 2. Uniaxial bilinear elastic-plastic law with kinematic hardening for steel rebars under cyclic loading (a) and uniaxial damage law of La Borderie with opening/closing of cracks (b).

The steel rebars are modelled by using a bilinear elastic-plastic law with kinematic hardening (*cf.* Figure 2 (a)). Fe500 steel rebars are used for the reinforcement, with an elastic stiffness of 210 GPa, a yielding stress of 500 MPa and a strain hardening modulus of 1000 MPa. The concrete is modelled with a “unilateral” damage law of La Borderie (1991), commonly used to model quasi-brittle materials under dynamic or cyclic loadings (*cf.* Figure 2 (b)). The parameters of the law of La Borderie are defined by considering an elastic stiffness of 31 GPa, a yielding tensile stress of 3.5 MPa, a yielding compressive stress of  $-10$  MPa and a crack reclosing stress of  $-3.5$  MPa.

### 3 TIME INTEGRATION SCHEME

Hybrid tests consist in linking a simulated numerical substructure to a tested specimen. An efficient substructuring technique is thus required to introduce the measured restoring forces to the numerical substructure and a non-iterative and unconditionally stable integration scheme dissipating high-frequency content due to the measures on the experimental setup (avoiding the risk of overshoot, *i.e.* collapse of the specimen).

Several time-integration schemes were used in the literature to solve the spatially discrete equation of motion (1) during hybrid tests.

$$\begin{aligned} \mathbf{M} \cdot \ddot{\mathbf{u}}(t) + \mathbf{C} \cdot \dot{\mathbf{u}}(t) + \mathbf{r}(\mathbf{u}(t)) &= \mathbf{F}(t) \\ \mathbf{F}(t) &= -\mathbf{M} \cdot \boldsymbol{\Gamma} \cdot \ddot{\mathbf{u}}_g(t) \end{aligned} \quad (1)$$

where  $\mathbf{M}$  is the mass matrix,  $\mathbf{C}$  the damping matrix,  $\mathbf{r}(\mathbf{u}(t))$  the restoring force vector,  $\mathbf{F}(t)$  the external force vector,  $\boldsymbol{\Gamma}$  the vector used to select the direction of the earthquake at the level of each DOF,  $\ddot{\mathbf{u}}_g(t)$  the ground acceleration, and  $\mathbf{u}(t)$ ,  $\dot{\mathbf{u}}(t)$  and  $\ddot{\mathbf{u}}(t)$  the displacement, velocity and acceleration vectors.

Some authors, such as Shing (1991), chose to use an implicit scheme based on the Hilber-Hughes-Taylor (HHT) method (Hilber et al 1977), also called  $\alpha$ -method. The equation of motion is solved at time  $(n + 1 + \alpha)$  where  $\alpha$  is a parameter usually set between  $-1/3$  and 0. This scheme is implicit since  $\mathbf{u}_{n+1}$  depends on  $\dot{\mathbf{u}}_{n+1}$ . The restoring force vector  $\mathbf{r}_{n+1}(\mathbf{u}_{n+1})$  being a function of  $\mathbf{u}_{n+1}$ , an iterative procedure is thus required to solve (1). This approach was successfully used by Shing (1991) to perform PsD tests. However, in the case of real-time or quick PsD hybrid tests, non-iterative time-integration schemes are used instead to decrease CPU time and the risk of overshoot. To maintain the stability of implicit schemes without iterating, Nakashima (1992) proposed to use an operator splitting (OS) method, based on a linear approximation of the restoring force vector (2).

$$\begin{aligned} \mathbf{r}_{n+1}(\mathbf{u}_{n+1}) &\cong \mathbf{K}_I \cdot \mathbf{u}_{n+1} \\ &+ (\tilde{\mathbf{r}}_{n+1}(\tilde{\mathbf{u}}_{n+1}) - \mathbf{K}_I \cdot \tilde{\mathbf{u}}_{n+1}) \end{aligned} \quad (2)$$

where  $\mathbf{K}_I$  is a secant or tangent stiffness matrix, chosen to be as close as possible to the elastic stiffness matrix  $\mathbf{K}_E$  (for the sake of stability), and  $\mathbf{r}_{n+1}(\tilde{\mathbf{u}}_{n+1})$  the prediction of the restoring force vector (Combesure 1997). The system of linear equations to solve in order to compute  $\ddot{\mathbf{u}}_{n+1}$  is thus given in (3).

$$\widehat{\mathbf{M}} \cdot \ddot{\mathbf{u}}_{n+1} = \widehat{\mathbf{F}}_{n+1+\alpha} \quad (3)$$

where  $\widehat{\mathbf{M}}$  is the pseudo mass matrix (4), and  $\widehat{\mathbf{F}}_{n+1+\alpha}$  the pseudo force vector (5).

$$\widehat{\mathbf{M}} = \mathbf{M} + \gamma \cdot \Delta t \cdot (1 + \alpha) \cdot \mathbf{C} + \beta \cdot \Delta t^2 \cdot (1 + \alpha) \cdot \mathbf{K}_I \quad (4)$$

$$\begin{aligned} \widehat{\mathbf{F}}_{n+1+\alpha} &= (1 + \alpha) \cdot \mathbf{F}_{n+1} - \alpha \cdot \mathbf{F}_n \\ &+ \alpha \cdot \mathbf{r}_n - (1 + \alpha) \cdot \tilde{\mathbf{r}}_{n+1} \\ &+ \alpha \cdot \mathbf{C} \cdot \tilde{\dot{\mathbf{u}}}_n - (1 + \alpha) \cdot \mathbf{C} \cdot \tilde{\dot{\mathbf{u}}}_{n+1} \\ &+ \alpha \cdot (\gamma \cdot \Delta t \cdot \mathbf{C} + \beta \cdot \Delta t^2 \cdot \mathbf{K}_I) \cdot \ddot{\mathbf{u}}_n \end{aligned} \quad (5)$$

Note that  $\tilde{\mathbf{u}}$  and  $\tilde{\dot{\mathbf{u}}}$  are the explicit predictions of the displacement and velocity vectors (6), and  $\beta$  and  $\gamma$

are the parameters of the time-integration scheme of Newmark, defined according to the  $\alpha$  parameter (7).

$$\begin{aligned}\tilde{\mathbf{u}}_{n+1} &= \mathbf{u}_n + \Delta t \cdot \ddot{\mathbf{u}}_n + \Delta t^2 \cdot \left(\frac{1}{2} - \beta\right) \cdot \ddot{\mathbf{u}}_n \\ \tilde{\mathbf{u}}_{n+1} &= \ddot{\mathbf{u}}_n + \Delta t \cdot (1 - \gamma) \cdot \ddot{\mathbf{u}}_n\end{aligned}\quad (6)$$

$\alpha$  is used to dampen the high-frequency content, mainly introduced by the measures in the case of hybrid tests. Its value of commonly set at  $-0.05$  (Hilber et al. 1977).

$$\beta = \frac{(1 - \alpha)^2}{4} \&\gamma = \frac{(1 - 2 \cdot \alpha)}{2}\quad (7)$$

The  $\alpha$ -OS method is implicit in the linear phase and explicit in the nonlinear phase. As demonstrated by Combescure et al. (1995) in practical cases, the  $\alpha$ -OS method competes very well in terms of accuracy with iterative implementations of the  $\alpha$ -method, even if a residual error appears due to the approximation in (2). Note that the predictive restoring force vector  $\tilde{\mathbf{r}}_{n+1}(\tilde{\mathbf{u}}_{n+1})$  is assessed once per time step: it is thus not necessary to solve (6) in increments. In addition, since  $\mathbf{K}_J = \mathbf{K}_E$ , the matrix  $\widehat{\mathbf{M}}^{-1}$  is computed before entering the time step loop, decreasing CPU time.

#### 4 SUBSTRUCTURING METHOD

In the case of hybrid tests, numerical and experimental substructures are split to introduce the measured restoring forces as external loads on common DOFs. The complete structure is thus substructured, as described in the example in Figure 3.

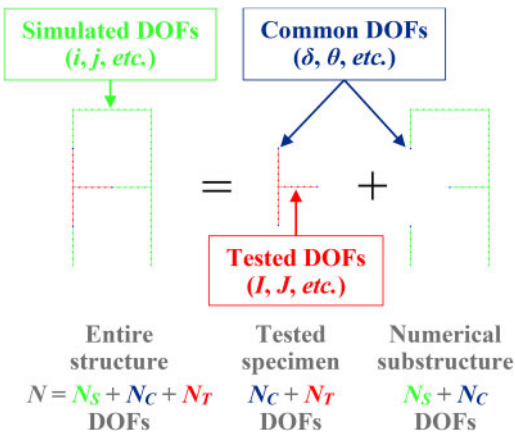


Figure 3. Substructuring of an in-plane two-storey frame: complete structure with 72 nodes, the tested specimen with 19 nodes, and numerical substructure with 56 nodes.

Among the  $N$  DOFs in the matrix system of (1),  $N_S$  DOFs only belong to the modelled substructure

(subscript  $i, j, etc.$ ),  $N_C$  belong to both the modelled substructure and the tested specimen (subscript  $\delta, \theta, etc.$ ) and  $N_T$  only belong to the tested specimen (subscript  $I, J, etc.$ ).

By distinguishing in (3) the systems of equations coming from the numerical substructure (subscripted  $S$ ) and the tested specimen (subscripted  $T$ ), it is possible to reorganize the matrix  $\widehat{\mathbf{M}}$  and the related terms as described in (8).

$$\begin{aligned}\begin{bmatrix} {}^S\widehat{\mathbf{M}}_{ij} & {}^S\widehat{\mathbf{M}}_{i\theta} & 0 \\ {}^S\widehat{\mathbf{M}}_{\delta j} & {}^S\widehat{\mathbf{M}}_{\delta\theta} + {}^T\widehat{\mathbf{M}}_{\delta\theta} & {}^T\widehat{\mathbf{M}}_{\delta J} \\ 0 & {}^T\widehat{\mathbf{M}}_{I\theta} & {}^T\widehat{\mathbf{M}}_{IJ} \end{bmatrix} \cdot \begin{bmatrix} \ddot{\mathbf{u}}_{i,n+1} \\ \ddot{\mathbf{u}}_{\theta,n+1} \\ \ddot{\mathbf{u}}_{J,n+1} \end{bmatrix} \\ = \begin{bmatrix} {}^S\widehat{\mathbf{F}}_{i,n+1+\alpha} \\ {}^S\widehat{\mathbf{F}}_{\delta,n+1+\alpha} + {}^T\widehat{\mathbf{F}}_{\delta,n+1+\alpha} \\ {}^T\widehat{\mathbf{F}}_{I,n+1+\alpha} \end{bmatrix}\end{aligned}\quad (8)$$

where  $\ddot{\mathbf{u}}_{i,n+1}$ ,  $\ddot{\mathbf{u}}_{\theta,n+1}$  and  $\ddot{\mathbf{u}}_{J,n+1}$  are the acceleration vectors respectively related to the simulated, common, and tested DOFs. So, by condensing the components of  $\ddot{\mathbf{u}}_{j,n+1}$ , (8) can be rewritten on the DOFs related to the tested specimen (9).

$$\begin{aligned}\begin{bmatrix} {}^T\widehat{\mathbf{M}}_{\delta\theta} + {}^S\widehat{\mathbf{M}}_{\delta\theta}^* & {}^T\widehat{\mathbf{M}}_{\delta J} \\ {}^T\widehat{\mathbf{M}}_{I\theta} & {}^T\widehat{\mathbf{M}}_{IJ} \end{bmatrix} \cdot \begin{bmatrix} \ddot{\mathbf{u}}_{\theta,n+1} \\ \ddot{\mathbf{u}}_{J,n+1} \end{bmatrix} \\ = \begin{bmatrix} {}^T\widehat{\mathbf{F}}_{\delta,n+1+\alpha} + {}^S\widehat{\mathbf{F}}_{\delta,n+1+\alpha}^* \\ {}^T\widehat{\mathbf{F}}_{I,n+1+\alpha} \end{bmatrix}\end{aligned}\quad (9)$$

where  ${}^S\widehat{\mathbf{M}}_{\delta\theta}^*$  and  ${}^S\widehat{\mathbf{F}}_{\delta,n+1+\alpha}^*$  are the condensed pseudo mass matrix and pseudo force vector defined in (10) & (11).

$${}^S\widehat{\mathbf{M}}_{\delta\theta}^* = {}^S\widehat{\mathbf{M}}_{\delta\theta} - {}^S\widehat{\mathbf{M}}_{\delta j} \cdot {}^S\widehat{\mathbf{M}}_{ij}^{-1} \cdot {}^S\widehat{\mathbf{M}}_{i\theta}\quad (10)$$

$${}^S\widehat{\mathbf{F}}_{\delta,n+1+\alpha}^* = {}^S\widehat{\mathbf{F}}_{\delta,n+1+\alpha} - {}^S\widehat{\mathbf{M}}_{\delta j} \cdot {}^S\widehat{\mathbf{M}}_{ij}^{-1} \cdot {}^S\widehat{\mathbf{F}}_{i,n+1+\alpha}\quad (11)$$

The measured restoring force vector  ${}^T\tilde{\mathbf{r}}_{\delta,n+1}$  is introduced in the pseudo force vector  ${}^T\widehat{\mathbf{F}}_{\delta,n+1+\alpha}$  (5), whereas the restoring force vectors computed on the numerical substructure  ${}^S\tilde{\mathbf{r}}_{i,n+1}$  and  ${}^S\tilde{\mathbf{r}}_{\delta,n+1}$  are introduced in  ${}^S\widehat{\mathbf{F}}_{i,n+1+\alpha}$  and  ${}^S\widehat{\mathbf{F}}_{\delta,n+1+\alpha}$ .

Note that the components related to the internal tested DOFs (indexed  $I, J$  in Figure 3) are computed by modelling the tested specimen. The same finite elements and nonlinear material laws are usually used on both the numerical and tested substructures. The elastic stiffness matrix of the tested specimen can be initially set based on measurements performed on the experimental setup. The displacement of the tested DOFs (stored in  ${}^T\widehat{\mathbf{u}}_{J,n+1}$ ) can either be predicted or measured at the level of the neutral axis (by using field measurements or interpolation methods). Knowing the values of the reactions applied to the common DOFs,

it is thus possible to approximate the restoring force vector  $\tilde{r}_{j,n+1}$  as well as the displacements of the tested specimen under earthquake (stored in  ${}^T\mathbf{u}_{j,n+1}$ ).

At the time step  $(n+1)$ , (9) is firstly solved to compute the acceleration vector on the common DOFs. Once  $\ddot{\mathbf{u}}_{\theta,n+1}$  is known, the acceleration vector related to the simulated DOFs (named  $\ddot{\mathbf{u}}_{j,n+1}$ ) is then assessed by solving (12).

$${}^S\widehat{\mathbf{M}}_{ij} \cdot \ddot{\mathbf{u}}_{j,n+1} = {}^{SC}\widehat{\mathbf{F}}_{n+1+\alpha} \quad (12)$$

where  ${}^{SC}\widehat{\mathbf{F}}_{n+1+\alpha}$  is the condensed pseudo force vector defined in (13).

$${}^{SC}\widehat{\mathbf{F}}_{n+1+\alpha} = {}^S\widehat{\mathbf{F}}_{i,n+1+\alpha} - {}^S\widehat{\mathbf{M}}_{i\theta} \cdot \ddot{\mathbf{u}}_{\theta,n+1} \quad (13)$$

During hybrid tests, (9) and (12) are solved on two computers exchanging data, decreasing CPU time. The first one (called master PsD computer) is responsible for the tested specimen. It sends instructions to the experimental setup and receives measures. It ensures the analogue to digital (A/D) conversion of data with the help of an acquisition card and computes the acceleration vector  $\ddot{\mathbf{u}}_{\theta,n+1}$  by solving (9). The second computer is responsible for the modelled substructure and computes the acceleration vector  $\ddot{\mathbf{u}}_{j,n+1}$ , according to (12).

## 5 REDUCED ORDER MODELLING BY USING A POD-ROM METHOD

In the case of hybrid tests, solving nonlinear substructures at each time step increases CPU time, even if a non-iterative time-integration scheme is used. Carrying these tests in real-time can thus be difficult due to the additional delay of the actuators, especially when the numerical substructure is modelled with a high number of DOFs. In the literature, most of the researchers use either a linear model (Bonnet et al. 2008) or nonlinear macroelements (Moutoussamy 2013). Other methods need to be used to reduce the CPU time with many DOFs and nonlinear material laws during the online phase (*i.e.* during hybrid tests). Among them, the POD-ROM method allows reducing the size of matrix systems by projecting equations on a basis made of few nonlinear POD-modes.

The key idea is to perform first a full offline step-by-step nonlinear analysis on the complete structure (including both numerical and tested substructures). Snapshots are then extracted from the results to compute  $N$  nonlinear POD-modes by using a Singular Value Decomposition (SVD) procedure (with  $N$  the number of DOFs).  $m$  POD-modes are then selected to build a modal projection basis. This reduces the number of DOFs and decreases CPU time during the online phase. The displacement vectors  $\mathbf{u}_j(t)$  (related to the simulated DOFs) can thus be expressed in a new basis  $\Phi = [\varphi_1 \ \dots \ \varphi_m]$  of dimension  $m \ll N$  as described in (14).

$$\mathbf{u}_j(t) \cong \Phi \cdot \mathbf{q}(t) \quad (14)$$

where  $\mathbf{q}(t)$  is the vector of size  $m \times 1$  containing the coordinates of displacements in the new basis  $\Phi$  and  $\varphi_{i=1,\dots,m}$  the POD-modes computed from a SVD procedure. So, by substituting  $\ddot{\mathbf{u}}_{j,n+1}$  with  $\ddot{\mathbf{q}}_{n+1}$  in (12), it comes:

$$\Phi^T \cdot {}^S\widehat{\mathbf{M}}_{ij} \cdot \Phi \cdot \ddot{\mathbf{q}}_{j,n+1} = \Phi^T \cdot {}^{SC}\widehat{\mathbf{F}}_{n+1+\alpha} \quad (15)$$

Note that when the  $\alpha$ -OS time-integration scheme is used, operator  $\Phi^T \cdot {}^S\widehat{\mathbf{M}}_{ij} \cdot \Phi$  is computed once and set as a constant during the online phase. However, the nonlinear restoring force vectors  ${}^S\mathbf{r}_{n+1}$  always needs to be computed in the full coordinates, making this operation the most time-consuming part of the entire process. The use of a non-iterative  $\alpha$ -OS method is thus relevant to avoid multiple reassessments of  ${}^S\mathbf{r}_{n+1}$  at each time step.

## 6 APPLICATION

### 6.1 Case study

One of the aims of this paper is to propose a PsD hybrid experimental set that allows for assessing the behaviour of a RC column/beam junction under earthquake. In the following, all the simulations are performed using the ground x-acceleration drawn in Figure 4. It is an artificial signal typical of a French average (close to strong) seismic hazard area. Its peak average (close to strong) seismic hazard area. Its peak ground acceleration (PGA) equals  $2.32 \text{ m/s}^2$  and is reached at time 3.16 s.

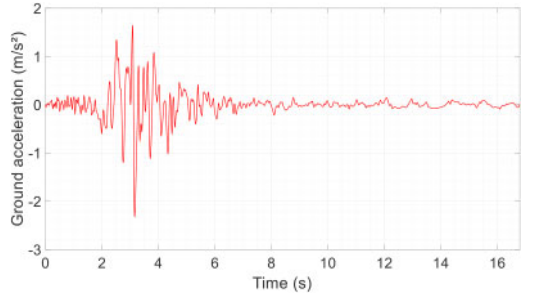


Figure 4. Ground acceleration versus time.

The case study is a three-storey RC frame of 3 m long spans and 3 m high storeys (*cf.* Figure 5). All the columns are fixed to the foundation level and have a  $15 \times 15 \text{ cm}$  square cross-section, while the beams have a  $15 \times 25 \text{ cm}$  rectangular one. The diameter of each longitudinal steel rebar is set at 12 mm, and the steel coating is equal to 20 mm (*cf.* Figure 6 (a)). A mass per unit of length equal to  $900 \text{ kg/m}$  is applied to each floor *via* the longitudinal beams (live loads), in addition to the dead loads. The last storey is two-span long, while the others are made of four spans: a rooftop is thus located at the 2nd-floor level. As a result, the masses and the dead loads are the highest on the 1st-floor column/beam junction located on the western side of the building. This structural element is thus assumed as the tested specimen in the following.

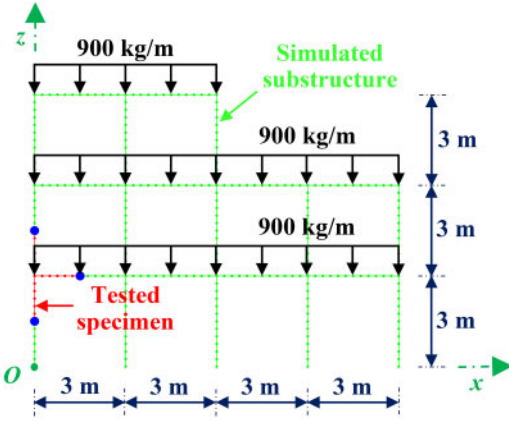


Figure 5. Elevation view of the three-storey RC frame.

A viscous damping ratio set at 2% at  $f_1 = 1.19$  Hz (*i.e.* the main eigenfrequency) is applied to dampen the high-frequency content. The damping matrix is thus defined such as  $C = \beta_M \cdot K_E$ , with  $\beta_M = 0.02 / (\pi \cdot f_1)$ , *i.e.*  $\beta_M = 5.3 \times 10^{-3}$  s/rad. Several researchers showed from experiments that this damping matrix is well suited to model damaging reinforced concrete structures, knowing that the damping cannot depend on the mass matrix when the section is fully broken (Faria 2002). The damping is thus managed by the concrete damage in the low-frequency range.

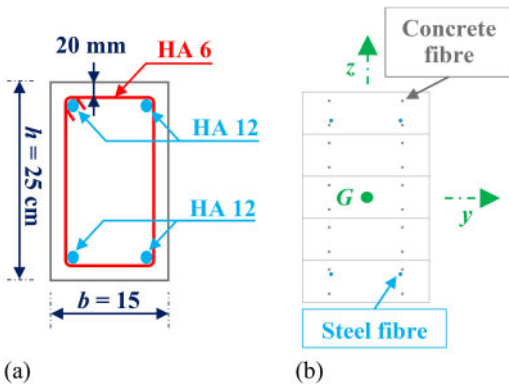


Figure 6. Cross-section of the beams (a) and mesh of the cross-section of the beams (b).

The complete structure comprises 798 free DOFs (*i.e.* 271 nodes), while all the cross-sections are divided into  $1 \times 5$  surface elements. The concrete fibres are located at the integration points of the surface elements (grey dots), while the steel fibres (blue dots) are located at 32 mm from the edges of the cross-sections (*cf.* Figure 6 (b)).

During the hybrid test, the restoring forces applied to the common DOFs (see blue dots in Figure 5) are measured on a specimen of the columns/beam junction. Thus, relevant boundary conditions need to be applied to the experimental setup to achieve viable results, as described in Section 6.2.

## 6.2 Virtual experimental setup

The column/beam junction includes the mid-length of the right beam and the mid-heights of the upper and lower columns. Even if all ends are embedded in an actual structure, several simplifications can be assumed on the experimental setup based on the properties of the building as well as the loading applied on it.

Firstly, it is commonly assumed in earthquake engineering that the mass of the building is mainly located at floor level. As a result, the bending moment evolves linearly along the columns when horizontal forces are applied to the floors, as it is the case during earthquakes. So, the bending moment can be considered as close to zero at mid-height of the storeys (as shown in Figure 7 (b)). Pin connections are thus applied at the ends of the half-columns on the tested specimen, allowing them to rotate freely.

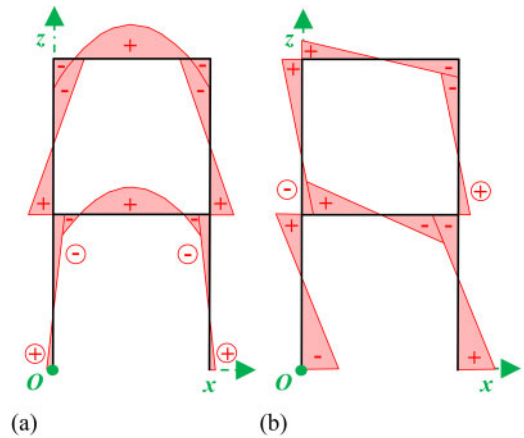


Figure 7. Distribution of the bending moment on a two-storey frame under vertical live loads (a) and horizontal earthquake (b).

Secondly, by considering that the PGA of the ground acceleration in Figure 4 (equal to  $2.16 \text{ m/s}^2$ ) is more than four times lower than the gravitational acceleration (equal to  $9.81 \text{ m/s}^2$ ), it is reasonable to consider that the horizontal earthquake has a low influence on the vertical displacements of the spans (compared to the dead and live loads). As a result, the beams are mainly loaded by the vertical live loads, so the bending moment reaches an extremum close to the mid-length of the spans (*cf.* Figure 7 (a)). The end of the half-beam is thus not able to rotate on the experimental setup.

Vertical and horizontal displacements  $U_{x1}$ ,  $U_{x2}$  and  $U_{z2}$  are applied at the ends of the upper half column and half beam by using three actuators (*cf.* Figure 8).  $F_{z1}$  is applied at the top of the upper half column by using pre-stressed steel rebars. Its value is set as a constant and equal to 27.8 kN according to the dead and live loads (the earthquake is thus neglected).

The live loads are applied to the half beam by using an additional static actuator. Knowing that the mass per unit length is 900 kg/m and that the half beam is

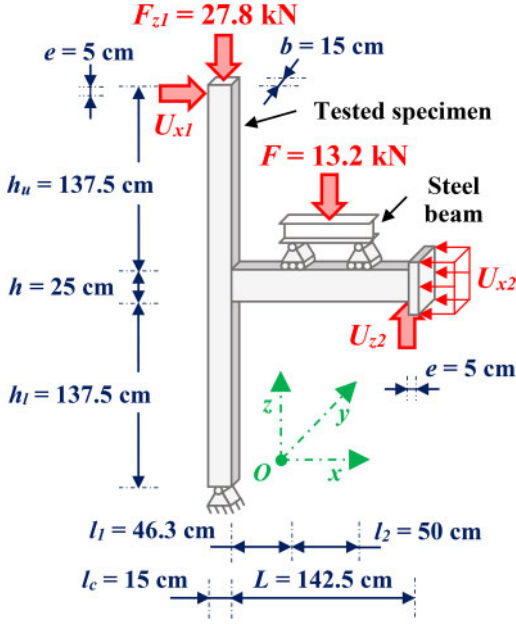


Figure 8. Elevation view of the three-storey RC frame.

1.5 m long, the force applied by this actuator is equal to 13.2 kN. This vertical load is transmitted to the half beam *via* a 50 cm long simply supported steel beam. The forces  $F_{x3}$  and  $F_{z3}$  (applied to the pin connection at the end of the lower half column) are measured, whereas the moment  $M_{y2}$  at the end of the half beam can be assessed by writing the equilibrium of the tested specimen.

As a result, the restoring forces vector  $T\hat{r}_\delta$  related to the common DOFs has seven non-zero components:  $F_{x1}, F_{z1}, F_{x2}, F_{z2}, M_{y2}, F_{x3}, F_{z3}$ . Note that this experimental setup is complex but realistic. If necessary, the vertical live load  $F = 13.2$  kN can be reasonably neglected on the span linked to the column/beam junction (on both substructures).

### 6.3 Numerical modelling of the experimental setup

Before performing the PsD hybrid test, a detailed finite elements analysis is firstly required to set the properties of the actuators (strength, stroke, ...) as well as to check the reliability of the boundary conditions detailed in Section 6.2. To do so, the tested specimen is replaced by a 2D numerical model of the column/beam junction defined in Cast3M<sup>®</sup> software.

Here, the concrete is modelled by using 980 quadratic surface elements, while the steel rebars are made of 624 uniaxial rods whose properties are defined per unit of length (*cf.* Figure 9). The transverse steel rebars are explicitly modelled, contrary to the multifibre beam elements. Their spacing varies between 5 and 15 cm. They are mainly placed at the ends of the specimen and at the level of the connection between the beam and the columns (to avoid the

appearance of shearing collapse mechanisms in case of earthquake). The area of the longitudinal steel rebars is equal to 15.1 cm<sup>2</sup>/m, while it is set at 8.3 cm<sup>2</sup>/m for the transverse ones.

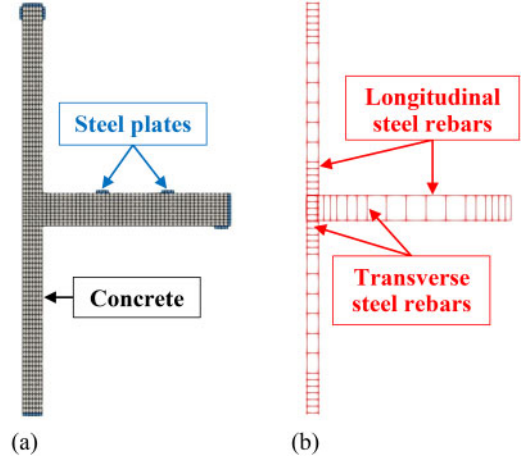


Figure 9. Elevation view of the 2D mesh of the tested specimen (a) and steel rebars (b) defined in Cast3M<sup>®</sup> software.

Note that 2.5 cm thick steel plates are located at the ends of the specimen and at the location of the actuators (as it is the case during actual experiments on RC structures). This avoids the appearance of local stress concentrations and prevents the concrete from tearing off.

The bilinear elastic-plastic law with kinematic hardening defined in Section 2.2 is used with the same parameters to model the behaviour of the steel rebars. The concrete is modelled by an accurate quasi-brittle material law available in Cast3M<sup>®</sup> software. The stiffness recovery, inelastic strains and frictional sliding are all considered (Richard et al. 2010). The law is defined by considering an elastic stiffness of 31 GPa, a yielding tensile stress of 3.5 MPa, a Poisson ratio of 0.2, a tension brittleness of  $1.10^{-2}$ , a compression brittleness of  $4.710^{-4}$ , a kinematic hardening of  $7.10^9$  Pa and a nonlinear hardening of  $7.10^{-7}$  Pa<sup>-1</sup>. Contrary to the La Borderie damage law, the energy dissipation due to frictional sliding is modelled, although the “unilateral” effect is partial (*cf.* Figure 10).

The finite element analysis is next performed on the simulated substructure (made of multifibre beam elements) by using a solver defined in MATLAB<sup>®</sup>, while the displacements of the actuators are sent to a console running Cast3M<sup>®</sup> software in parallel. Restoring forces are then computed and sent to MATLAB<sup>®</sup> for the next time step and so on. The analysis is first performed using the full order model (FOM). A POD projection modal basis is then added to the  $\alpha$ -OS solver, as described in Section 5. The results are compared and discussed in Section 6.4.

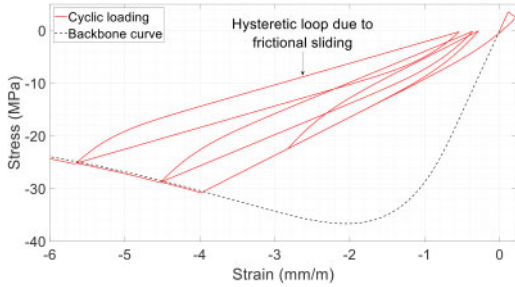


Figure 10. Uniaxial damage law of concrete under cyclic loading with partial “unilateral” effect and frictional sliding.

#### 6.4 Results with the full and reduced models

The numerical substructure is reduced by using a modal projection basis made of POD-modes computed from the results of an offline implicit finite element analysis performed on the entire structure.

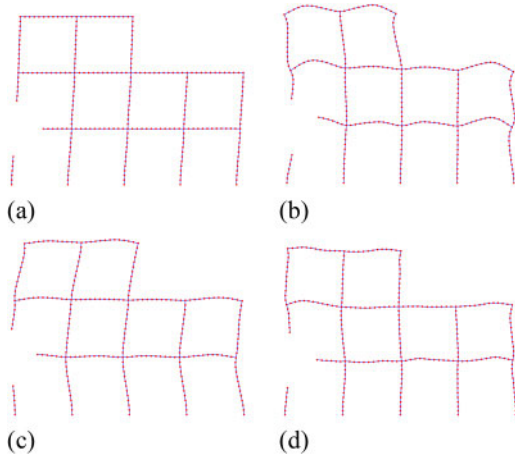


Figure 11. POD-modes of the numerical substructure: 1<sup>st</sup> mode (a), 2nd mode (b), 3rd mode (c) and 4th mode (d).

The use of POD-modes introduces additional information on the nonlinearities (*i.e.* location of damage and plasticity, as it is clearly visible in the shape of the 2nd POD-mode drawn in Figure 11 (b)) as well as the global response of the building, despite cutting part of the high-frequency content. As a result, their use to perform hybrid tests can change the displacements applied to the tested specimen and the response of the numerical substructure. To assess the reliability of the reduced-order model (ROM) in the framework of PsD hybrid tests, a comparison with the full order model (FOM) is thus necessary.

According to Ayoub (2021), the number of POD-modes can reasonably be assessed by guaranteeing that at least 99 % of the total system energy is considered for the ROM. Knowing that the singular value  $\Lambda_i$  indicates the amount of energy brought by the  $i^{\text{th}}$

POD-mode, the energy criterion used to assess  $m$  can thus be written as described in (16).

$$\frac{\sum_{i=1}^m \Lambda_i}{\sum_{j=1}^N \Lambda_j} \geq 0.99 \quad (16)$$

Figure 12 shows that this criterion is fully reached with  $m = 10$  POD-modes: this value is thus used to build the POD projection modal base related to the numerical substructure.

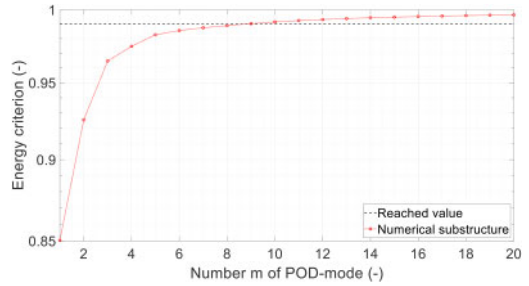


Figure 12. Energy criterion based on the singular values.

The displacement response is plotted in Figure 13 at times  $t = 4.78$  s and  $t = 5.38$  s (*i.e.* when the horizontal displacements reach their extrema during the strong motion phase). Results related to the implicit offline phase, hybrid test with the FOM and hybrid test with the ROM are compared. Note that the displacements of the tested specimen are plotted by post-processing, and that deformations are amplified by a factor 50.

The global responses of the RC frame computed in hybrid test conditions fit well with the implicit Newmark reference, despite the simplifications made on the boundary conditions applied to the tested specimen. However, with the FOM, note that the numerical model of the tested specimen undergoes lower deformations than the other RC column/beam junctions, leading to lower horizontal displacements on the complete structure, especially at the top of the building. On the contrary, the dynamic response is similar on all junctions with the ROM, leading to more consistent and “realistic” results, each POD-modes carries information about the local nonlinearities and the global response of the RC frame.

Simplifications being most of the times necessary on PsD experimental setups, these results show that using POD-modes computed from a fully numerical implicit finite element analysis carried out on the complete structure partially corrects the induced error and improves the consistency of the dynamic responses of both the numerical substructure and the tested specimen. However, it should be noted that the CPU time related to the numerical substructure (modelled on an Intel<sup>TM</sup> Core<sup>TM</sup> i9-10900K CPU @ and 64 GB RAM personal computer using MATLAB<sup>©</sup> software) is approximately equal to 42 s with the FOM and 40 s with the ROM. As a result, the number of DOFs is not high enough to save significant CPU time when

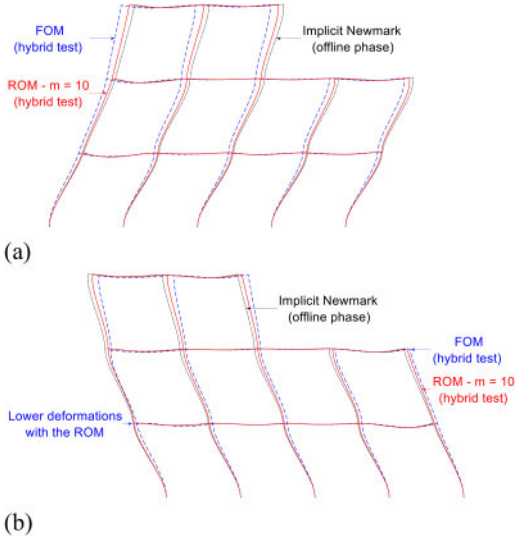


Figure 13. Response in displacements of the entire RC frame at times  $t = 4.78$  s (a) and  $t = 5.38$  s (b).

a POD projection modal base is used, the  $\alpha$ -OS time integration scheme is non-iterative and all operators are pre-computed. To save more CPU time and allow for faster testing, it is thus necessary to reduce the computational cost due to assessing the restoring force vector  ${}^S\tilde{\mathbf{r}}(u)$  at each time step. This can be achieved by using a POD Discrete Empirical Interpolation Method (DEIM) approach.

To ensure that the boundary conditions applied to the tested specimen lead to actual damage mechanisms, the distributions of the damage index computed with the FOM and the ROM are compared in Figure 14.

Contrary to the dynamic response of the full structure, the static response of the tested specimen is almost the same with the FOM and the ROM (*cf.* Figure 15). As a result, the same damage mechanisms appear. Damage index at time  $t = 2.60$  s shows that cracks due to bending first appear at the transverse steel rebars (where the reinforced concrete is locally stiffer). Then, at time  $t = 2.73$  s, shearing led to the appearance of a  $45^\circ$  inclined crack on the node connecting the columns to the beam. At the end of the hybrid test (*i.e.*  $t = 16.79$  s), damage is thus mainly located around these areas. These results are in accordance with the experiments performed by Masi et al. (2013), which highlighted similar damage mechanisms and shear/drift behaviour (*cf.* Figure 15). As a result, the boundary conditions applied to the specimen can be considered as well suited to perform hybrid tests on column/beam junctions.

The minimum requirements to consider for the actuators applying the displacements  $U_{x1}$ ,  $U_{x2}$  and  $U_{z2}$  are finally assessed based on the previous results. Note that the data given in Table 1 will be soon used to perform an actual PsD hybrid test on a column/beam junction.

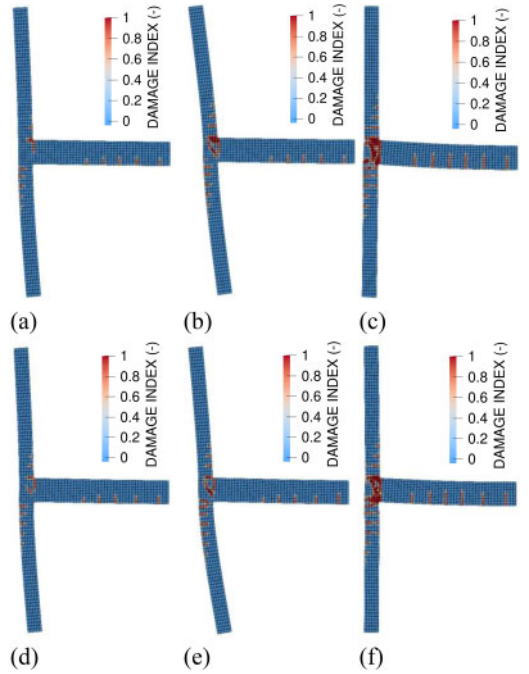


Figure 14. Damage index of specimen: FOM at times  $t = 2.60$  s (a),  $t = 2.73$  s (b) and  $t = 16.79$  s (c), and ROM ( $m = 10$ ) at times  $t = 2.60$  s (d),  $t = 2.73$  s (e) and  $t = 16.79$  s (f).

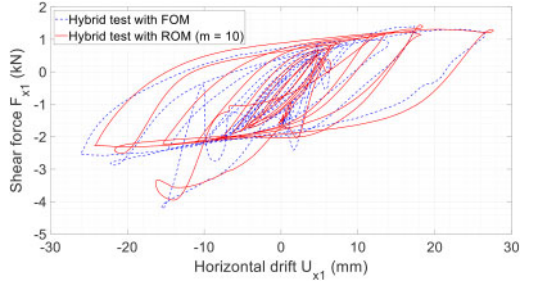


Figure 15. Shear/drift response of the tested specimen.

Table 1. Minimum requirements to consider for the actuators.

Displacement	Strength kN	Stroke mm	Type
$U_{x1}$	4.2	52.6	Double acting
$U_{x2}$	4.6	28.9	Double acting
$U_{z2}$	9.0	2.7	Simple acting

## 7 CONCLUSIONS

In this paper, a PsD hybrid experimental setup allows for assessing the nonlinear behaviour of a RC column/beam junction under earthquake is proposed.

Pins connections are applied to the ends of the half-columns, while the rotations are not allowed at the end of the half beam. The static loads applied to the upper storeys are modelled by pre-stressing the half-columns with steel rebars, while the displacements at the ends of the tested specimen are applied by using three actuators. The numerical substructure is modelled by using nonlinear multifibre beam elements, and the use of a POD projection modal basis to reduce its computational cost is investigated. FEM analyses are carried in hybrid test conditions by substituting the tested specimen with a numerical model defined in Cast3M<sup>®</sup> software.

Results showed that using a POD projection modal basis computed from an offline implicit finite element analysis improves the consistency of the response of both numerical and tested substructures (additional information on the global response of the structure as well as nonlinearities being added) but does not significantly reduce the CPU time. In addition, the simplified boundary conditions applied to the specimen led to actual damage mechanisms, showing their relevancy.

To reduce the computational cost due to the assessment of the restoring force vector  $S_{\mathbf{r}_i}(\mathbf{u}_j)$ , further investigations are led to assess the reliability of the POD-DEIM hyper reduction method in the framework of PsD hybrid tests.

## REFERENCES

- Ayoub, N., Larbi, W., Pais, J., Rouleau, L., & Deü, J.-F. 2021. An application of the proper orthogonal decomposition method or nonlinear dynamic analysis of reinforced concrete structures subjected to earthquakes. *COMPADYN 2021, 8th ECCOMAS Thematic Conference on Computational Methods and Structural Dynamics and Earthquake Engineering*. Athens, Greece.
- Bonnet, P., Williams, M., & Blakeborough, A. 2008. Evaluation of numerical time-integration schemes for real-time hybrid testing. *Earthquake Engineering and Structural Dynamics*, 37:1467–1490.
- Buchet, P., & Pegon, P. 1994. PsD testing with substructuring: Implementation and use. *Special publication, ISPRA, I, 94.25*.
- Combescuré, D., & Pegon, P. 1997.  $\alpha$ -operator splitting time integration technique for pseudodynamic testing. error propagation analysis. *Soil Dynamic and Earthquake Engineering*, 16:427–443.
- Combescuré, D., Pegon, P., & Magonette, G. 1995. Numerical investigation of the impact of experimental errors on various pseudo-dynamic integration algorithms. *Proceeding of the 10th European Conference on Earthquake Engineering* (pp. 2479–2484). Rotterdam, The Netherlands: Duma G. (ed.) Balkema.
- Faria, R., Vila Pouca, N., & Delgado, R. 2002. Seismic behavior of a r/c wall: numerical simulation and experimental validation. *Journal of Earthquake Engineering*, 6(4):473–498.
- Hakuno, M., Shidawara, M., & Hara, T. 1969. Dynamic destructive of a cantilever beam controlled by an analog-computer. *In Proceedings of JSCE*, n°171.
- Hilber, H., Huges, T., & Taylor, R. 1977. Improved numerical dissipation for time integration algorithms in structural dynamics. *Earthquake Engineering and Structural Dynamics*, 5(3):282–292.
- Iskef, A. 2016. Technologies informatiques pour l'étude du comportement expérimental et numérique d'un assemblage poteau-poutre en béton armé. *PhD Thesis. ENS Cachan. (In French)*.
- Kotronis, P., Davenne, L., & Mazars, J. 2004. Poutre multifibre de Timoshenko pour la modélisation de structures en béton armé. Théorie et applications numériques. *Revue Française de Génie Civil, Taylor & Francis*, 8(2–3):329–343. (In French).
- La Borderie, C. 1991. Phénomènes unilatéraux dans un matériau endommageable: modélisation et application à l'analyse de structures en béton. *PhD Thesis. Paris VI University. (In French)*.
- Lebon, G. 2011. Analyse de l'endommagement des structures de Génie Civil : techniques de sous-structuration hybride couplées à un modèle d'endommagement anisotrope. *PhD Thesis, ENS Cachan. (In French)*.
- Masi, A., Santarsiero, G., Lignola, G., & Verderame, G. M. 2013. Study of the seismic behavior of external RC beam-column joints through experimental tests and numerical simulations. *Engineering Structures*, 52:207–219.
- Moutoussamy, L. 2013. Essais hybrides en temps réels sur structures de Génie Civil. *PhD Thesis. ENS Cachan. (In French)*.
- Nakashima, M., Kato, H., & Takaoka, E. 1992. Development of real-time pseudo dynamic testing. *Earthquake Engineering and Structural Dynamics*, 21(1):79–92.
- Nguyen, T. (2012). Analyses du comportement de rupteurs thermiques sous sollicitations sismiques. *PhD Thesis, ENS Cachan. (In French)*.
- Pegon, P., & Pinto, V. 2000. Pseudo-dynamic testing with substructuring at the ELSA Laboratory. *Earthquake Engineering and Structural Dynamics*, 29:905–925.
- Richard, B., Ragueneau, F., Cremona, C., & Adelaide, L. 2010. Isotropic continuum damage mechanics for concrete under cyclic loading: Stiffness recovery, inelastic strains, and frictional sliding. *Engineering Fracture Mechanics*, 1203–1223.
- Shing, P., Vannan, M., & Carter, E. (1991). Implicit time integration for pseudodynamic tests. *Earthquake Engineering and Structural Dynamics*, 20:551–576.
- Souid, A., Delaplace, A., Ragueneau, F., & Desmorat, R. 2009. Pseudo-dynamic testing and nonlinear substructuring of damaging structures under earthquake loading. *Engineering Structures*, 31(5):1102–1110.
- Takanashi, K., & Nakashima, M. 1987. Japanese activities on online testing. *Journal of Engineering Mechanics*, 113(7):1014–1032.